APPENDIX H:

ACOUSTIC CALIBRATION AND MODELING OF SEISMIC SOURCES ON THE RV *LANGSETH* (2007-2008)

APPENDIX H

ACOUSTIC CALIBRATION AND MODELING OF SEISMIC ACOUSTIC SOURCES ON THE R/V *LANGSETH* (2007-2008)

Introduction

Calibration of the 2-string and 4-string R/V *Langseth* seismic source arrays was carried out in the NW Gulf of Mexico during late 2007 and early 2008. One of the fundamental motivations for the *Langseth* calibration efforts was the need to assess and verify the accuracy and applicability of modeling the received sound levels of the array. The modeling has been used to predict the safety radii within which mitigation may be necessary in order to avoid exposing marine mammals to airgun sounds at levels where physical effects may occur. The amount of time available for the calibration work limited the number of parameters and configurations that could be tested, especially source towing depth. However, if the modeling can be verified for a few basic configurations, then it may be used to reliably predict the effects of small configuration changes.

Tolstoy et al. (2009) presented a description of the acquisition and analysis methods of the calibration study, as well as the initial results. Acoustic measurements were only obtained from the 4-string, 36-airgun array, which is typically used for 2-D seismic reflection and refraction surveys. Propagation measurements of pulses from the 4-string array were obtained in two of three water depths (~1600 m and 50 m) chosen for the calibration study. Additional work has recently been done on refining the navigation of the calibration buoy hydrophone at a third intermediate-depth slope site, as well as analysis of the 2-string array results, including its directivity and effects due to sub-seafloor interaction of sound waves at those sites (Diebold et al., in prep).

The results of the study showed that radii around the airguns for various received levels were larger in shallow water (Tolstoy et al. 2009). The results were presented using two metrics; SEL (sound exposure level, which is equivalent to energy flux density) and the 90% RMS values favored in the past for evaluation of behavioral responses of marine mammals to anthropogenic noise. Under certain circumstances, these two measures produce the same result, but for impulsive sources, including airgun arrays, 90% RMS is usually higher. As Madsen (2005) demonstrated, the exact difference is highly variable, depending on impulsivity, which may vary greatly for signals containing similar energy levels. Southall et al. (2007) have recommended that SEL be used instead, and we follow this practice here. In this appendix, we compare the modeling and calibration results.

Modeling *Langseth* Airgun Arrays for Mitigation

A simple raytrace-based modeling approach has been used to establish a priori safety radii for marine mammal mitigation during *Langseth* expeditions, and previously for the R/V *Ewing* (Tolstoy et al. 2004). One of the many motivating factors for the *Langseth* calibration efforts was to assess the accuracy of that modeling. Briefly, the modeling process is this:

1) Define the airgun array in terms of the size and relative location of each airgun [X, Y, and Z].
2) Model the near field signatures using Nucleus' MASOMO and extract them.
3) Decide upon a 2-D mesh of points, for example within a plane intersecting the center of the airgun array; a typical mesh is 100 x 50.
4) For each of the points in the mesh, create the signal that would be observed there when every airgun in the array was fired simultaneously.

5) For that signal, determine the desired statistic: Peak-to-peak dB, Peak dB, RMS dB, maximum psi, etc.
6) Contour the mesh.
7) Determine radii and the trajectory of maximum SPL from contour lines (Figure 1).

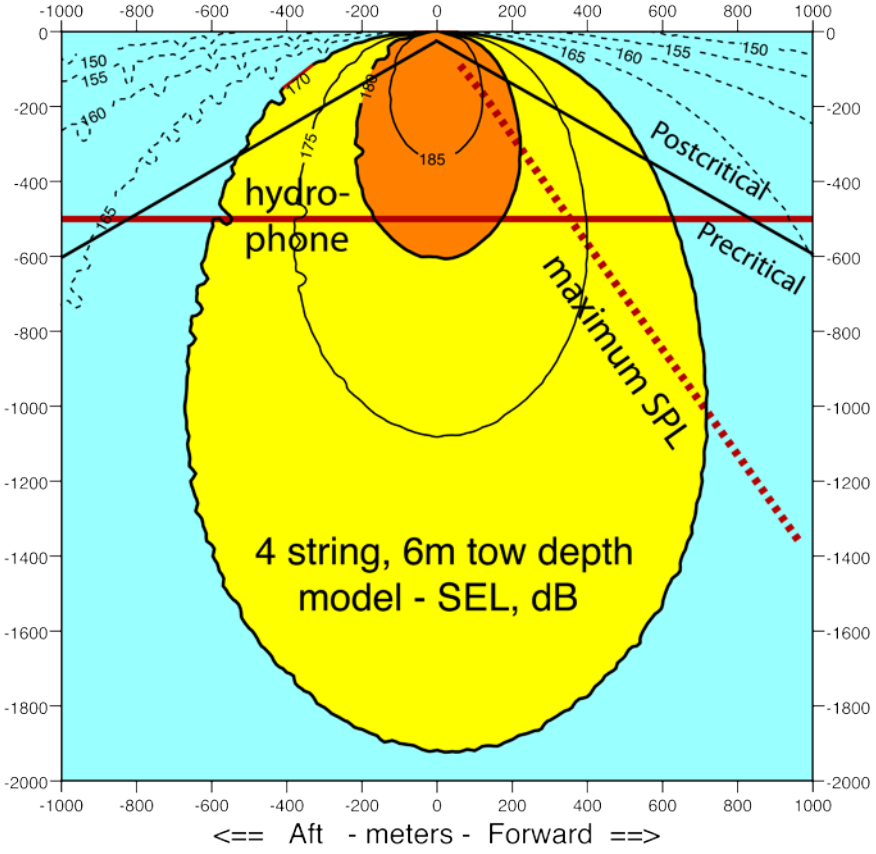

Figure 1. The direct-arrival model for *Langseth*'s 4-string airgun array, towed at 6 meters depth, the configuration used during the calibration procedure. While the calibration results should be compared to values modeled along the constant-depth "hydrophone" line, the maximum values, used for mitigation radii, are found along the slanted, dashed line. Energy which would be postcritically (i.e., totally) reflected or refracted at the sea floor propagates from the source and the sea surface in the field labeled "Postcritical." The angle of the dividing line separating pre-and-post critical depends on the velocity of sound below the seafloor, and the x-value of the point at which this line intersects the seafloor is called the "critical distance."

Most of the work lies in step 3 which has steps of its own:

a) For each of the airguns in the array, determine the distances, and thus the time-of-flight between the airgun and the mesh point, as well as the free surface ghost "image" of the airgun and the mesh point.
b) Scale and shift the airgun near field signal, dividing by the point-to-point distance and moving forward in time according to time-of-flight.
c) Scale and shift the near field signal's ghost image, as above, in addition multiplying by the free surface reflection coefficient [typically between -0.9 and -0.95]
d) Sum the results. For the *Langseth* 36-airgun array, 72 scaled and shifted signals are created and summed for each mesh point.

Comparing Modeling with Measurements

As illustrated in Figure 1, sound levels recorded by the calibration hydrophones (here located at a depth of 500 m) will not always be the maximum values as predicted by the model (max. SPL). Nonetheless, the modeling can be easily adapted to compare it directly with the calibration results (Figure 2)

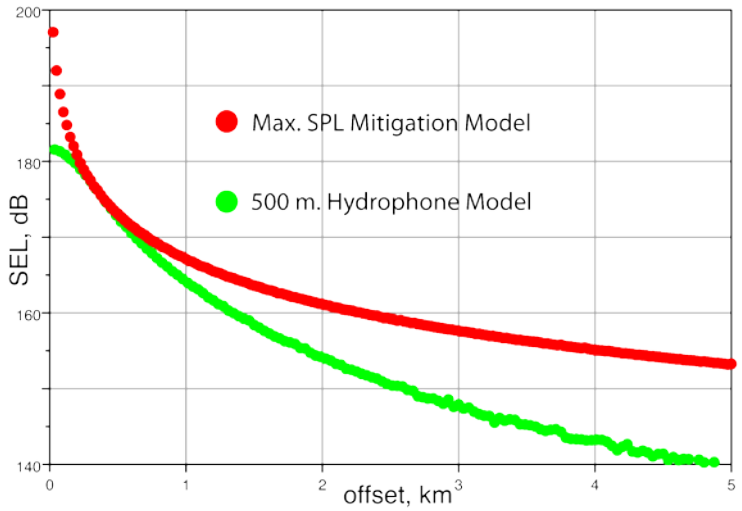

Figure 2. The modeled sound exposure levels along the "hydrophone depth" and "maximum SPL" lines drawn in Figure 1. The lower, green line should be compared to the calibration results, while the upper red line has been used to establish mitigation radii.

Deep site, bottom interaction

Results for the 4-string deep site *direct* arrivals were presented by Tolstoy et al. (2009). Direct and sea floor interacting arrivals were separated by windowing. In Figure 3, we present a summary plot for the 4-string source array at the deep calibration site, comparing *all* arrival amplitudes to the maximum direct-arrival mitigation model values. Water depth at this site averaged 1560 m, and the critical distance is about 5 km, although reflected arrivals (perhaps including energy postcritically returned from deeper, faster sedimentary layers) outweigh the direct arrivals at offsets greater than 2.5 km. An important observation is that along with the direct arrival amplitudes, all of the reflected and refracted arrival amplitudes fall below the direct-arrival mitigation model. It is also clear that the exact amplitudes of the precritical reflections between zero and 5 km are dependent upon details in the seafloor topography. The amplitudes of arrivals in this "precritical" zone also depend greatly upon the exact velocity structure at and below the seafloor. These amplitudes can be accurately predicted by modeling only with detailed and complete information of bathymetry and the subsurface.

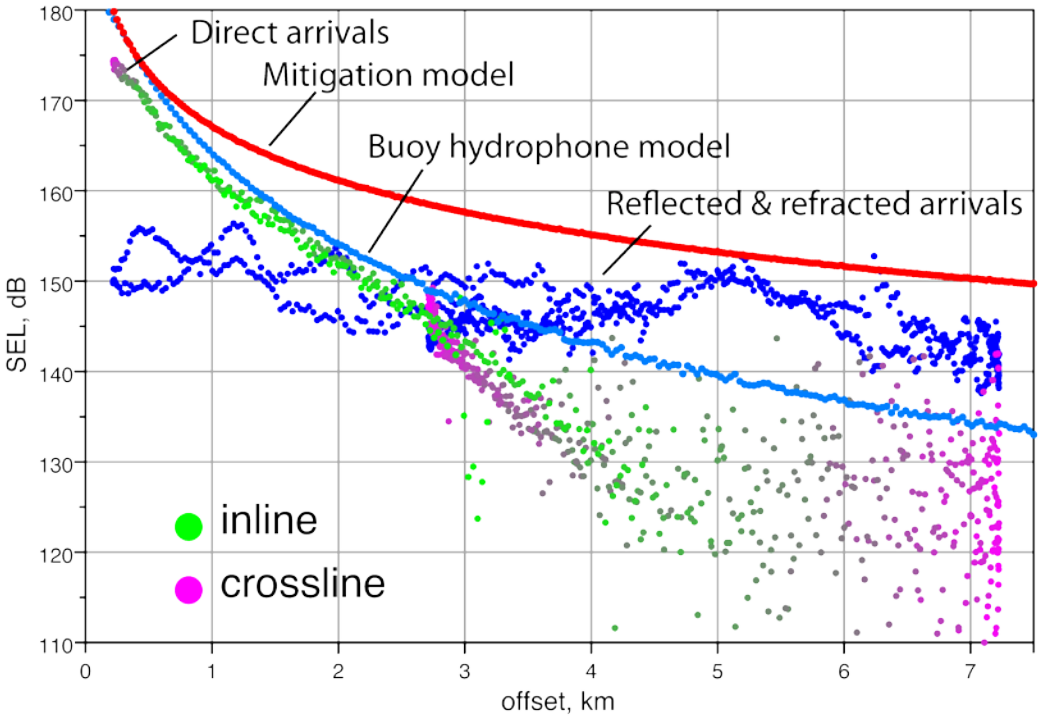

Figure 3. Energy flux levels for direct and reflected/refracted arrivals from the 4-string array at the deep calibration site. The maximum SPL, or "Mitigation" and "Buoy hydrophone" models do not include bottom interactions. The Buoy hydrophone model matches the observed direct arrival data very well, although it consistently over predicts amplitudes by a few dB.

Slope Site, 4-String Array, Intermediate Water Depth, Up-And-Down-Dip Variations

Data from the slope site, where only the full, 4-string array was tested, were not presented by Tolstoy et al. (2009). What is important about this site is that the data were acquired in intermediate (600–1100 m) water depths, with a sloping sea floor.

The direct arrival amplitudes for this site are very similar to those observed at the deep site for the 4-string array. Figure 4 shows these levels, compared to those predicted by modeling. The fit is good, except at near offsets, where the model under predicts the observed source levels. This situation is the opposite of the observations at the deep site (Figure 3, and Tolstoy et al. 2009) where the length and breadth of the source array produces a near-field effect resulting in a diminution in source levels at close proximity. A logical hypothesis is that the inter-string spacing was smaller than intended during the slope site close approaches, but due to the lack of complete GPS positioning on the array strings (the calibration was carried out before this system was perfected), this cannot be verified. As in the deep site case (Figure 3) measured levels fall well below predictions at offsets greater than 2.5 km, due to the downward-focusing sound velocity profile.

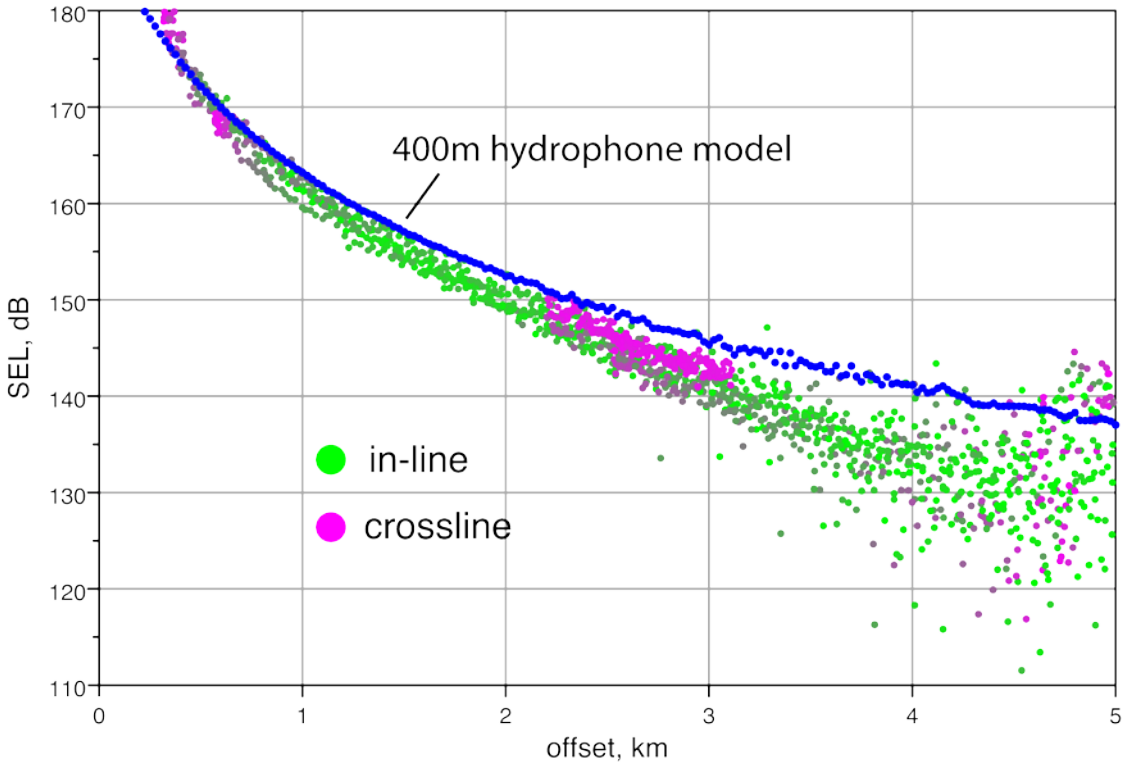

Figure 4. Energy flux density (SEL) values for direct arrivals at the slope site. In-line and cross-line aspects are color-coded. The 4-string model with 6-m tow depth and receiver depth of 400-m is shown for comparison. The model is only exceeded by the data at small offsets, and at large offsets where the direct arrival windowing started to fail.

In Figure 5, energy levels for seafloor-reflected and subseafloor-refracted arrivals are superimposed on the direct arrival levels. At this intermediate-depth (bathymetry varied from 600-1100 m) site, the crossover is located at 2 km offset, compared to 2.5 km at the deep site. An increase in amplitude, corresponding to the critical distance, beyond which postcritically reflected and refracted arrivals are generated, is seen at about 4 km (5 km for the deep site). The singular excursion observed as peaking at 2.9 km is certainly due to seafloor topography, though the exact cause was not determined. There is a notable bifurcation of levels for the bottom-interacting arrivals at source-receiver offsets greater than 5 km.

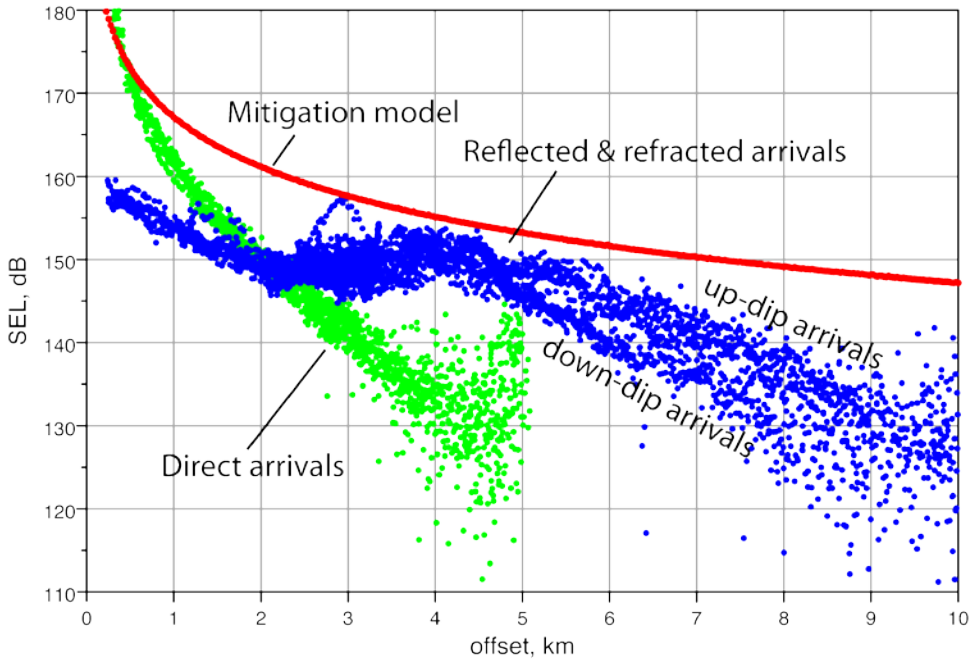

Figure 5. As in Figure 3, measured levels for seafloor reflected and sub-seafloor refracted arrivals are superimposed on the direct arrival values. Since the water is shallower at this site, the critical distance is 4 km, rather than the 5 km observed at the deep site. All observed levels (except at very near offsets) fall below the mitigation model predictions.

It is clear in Figure 5 that the reflected and refracted arrival amplitudes with source-receiver offsets greater than about 5 km fall along two diverging trajectories. When the source and receiver locations where these trajectories are best defined were identified, it was clear that the differences correspond to the source-receiver geometry in relation to the sloping bathymetry at this calibration site.

Average water depth for the down-dip shots was 800 m, compared to 1,050 m for the up-dip shots. Despite this difference, the critical distance for both sets of shots is about the same; 3.5–4 km. The reason for this is the sloping seafloor. When shooting up-dip, rays are crowded towards the source, shortening the critical distance, while the opposite is true when shooting down-dip (Levin 1971; Diebold and Stoffa 1981). This variation in ray density is also responsible for the paradoxical distribution of amplitudes; up-dip arrivals in deeper (1,050 m) water are stronger than down-dip arrivals in shallower (800 m) water. In all cases, however, amplitudes fall below the direct-arrival mitigation model line.

Use of Modeling to Extrapolate Tow-Depth Effects

Direct-arrival modeling can be used to examine the isolated effects of changes in array configuration. In Figure 6, the towing depth of the *Langseth* 4-string source array is varied between 6 and 15 m. This encompasses the entire range of tow depths employed between 2000 and 2010. The differences between plotted values can be used to predict amplitude changes induced by various principal investigators' choices of tow depths, which are made for the purpose of best serving a particular scientific target.

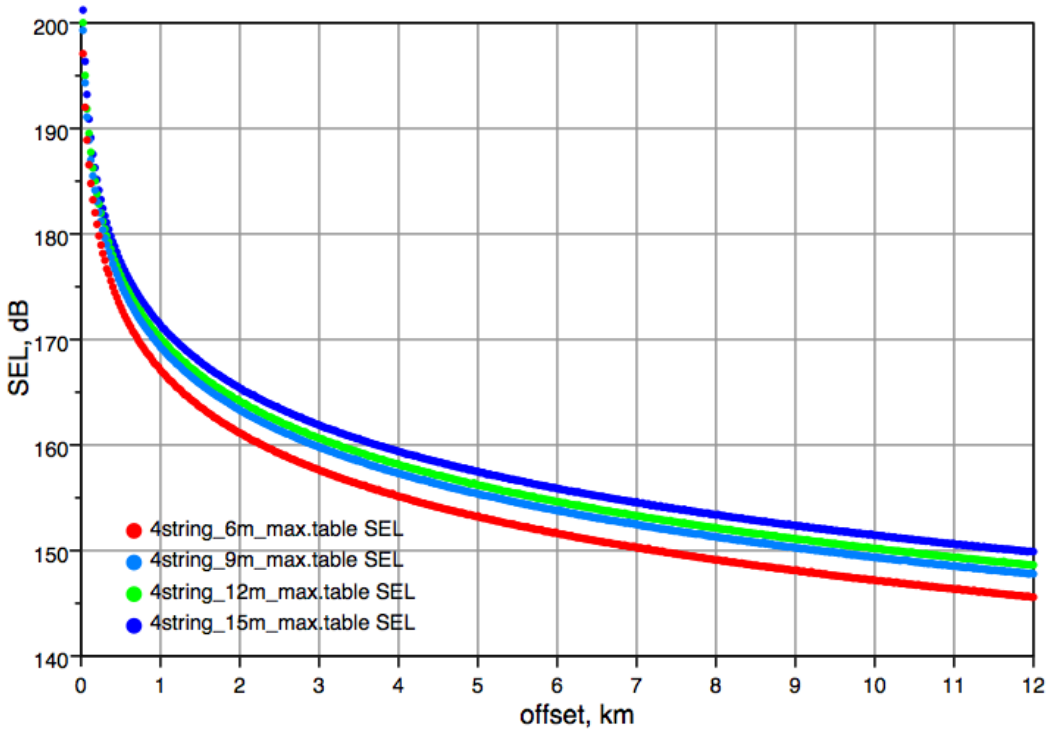

Figure 6. Direct-arrival modeling for the *Langseth* maximum 4-string source array as towed at four different depths. Lowest values correspond to the 6-m tow depth used during calibrations. Note that the increase in energy levels is not linear with increases in tow depth.

Conclusions

Comparison of the modeling and calibration results showed that the model represents the actual produced levels, particularly within the first few kilometers, where the predicted safety radii lie. At greater distances, local oceanographic variations begin to take effect, and the model tends to over predict. Since the modeling matches the observed measurement data quite well and can be used to predict maximum values, we argue that the modeling can continue to be used for defining mitigation radii, and further that it is valid for predicting mitigation radii for various tow depths.

References

Diebold, J.B. and P.L. Stoffa. 1981. The Traveltime equation, tau-p mapping and inversion of common midpoint data. Geophysics 46:238-254. [*reprinted* 1991: Slant-Stack Processing, G.H.F. Gardner & F.K. Levin eds. Geophysics Reprint Series 14:151-167.]

Levin, F. 1971. Apparent velocity from dipping interface reflections. Geophysics 36, 510; doi:10.1190/1.1440188

Madsen, P.T. 2005. Marine mammals and noise: Problems with root mean square sound pressure levels for transients. Journal of the Acoustical Society of America 117:3952-3957

Southall, B.L., A.E. Bowles, W.T. Ellison, J.J. Finneran, R.L. Gentry, C.R. Greene Jr., D. Kastak, D.R. Ketten, J.H. Miller, P.E. Nachtigall, W.J. Richardson, J.A. Thomas and P.L. Tyack. 2007. Marine mammal noise exposure criteria: Initial scientific recommendations. Aquatic Mammals 33:1-521.

Tolstoy, M., J.B. Diebold, S.C. Webb, D.R. Bohnenstiehl, E. Chapp, R.C. Holmes and M. Rawson. 2004. Broadband calibration of R/V/ Ewing seismic sources. Geophysical Research Letters 31, L14310, doi: 10.1029/2004GL020234.

Tolstoy, M., J. Diebold, L. Doermann, S. Nooner, S.C. Webb, D.R. Bohnenstiehl, T.J. Crone, and R.C. Holmes. 2009. Broadband calibration of the R/V Marcus G. Langseth four-string seismic sources. Geochemistry Geophysics Geosystems 10, Q08011, doi:10.1029/2009GC002451.